Chapter 8

Optical Fibre Gratings for Chemical and Bio - Sensing

Xianfeng Chen

Additional information is available at the end of the chapter

http://dx.doi.org/10.5772/54242

1. Introduction

We live in an era of technological revolutions that continue to impact our lives and constantly redefine the breath of our social interactions. The past century has witnessed many technological breakthroughs, one of which is fibre optics. Due to the advantages of non-electromagnetic, light weight, flexibility, low-loss and high temperature tolerance, optical fibre gratings have been become one of the most important components in optical communications and optical sensing [1-7].

Fibre gratings are broadly classified into fibre Bragg gratings (FBGs) and long-period gratings (LPGs). The period of an FBG is approximately half a micrometer whereas the period of an LPG is typically several hundred micrometers. From the conventional coupled-mode theory, in an FBG the guided mode will be coupled to the corresponding backward mode [2, 3]. Contrary to the contradirectional coupling in FBGs, LPGs induce codirectional coupling in an optical fibre where the guided mode will be coupled to the cladding modes when the difference of their propagation constants is equal to the corresponding spatial frequency. FBGs have been demonstrated to measure a wide range of physical parameters including temperature, strain, pressure, loading, bending and vibration [6, 7]. LPGs, as core to cladding modes forward-coupling devices, have been used as band-rejection filters, Erbium-doped fibre amplifier (EDFA) gain flatteners and as optical sensors to monitor strain, temperature, bending and surrounding-medium refractive index (SRI). Radiation-mode out coupling from tilted fibre gratings (TFGs) has also been demonstrated for applications in wavelength-division-multiplexing (WDM) channel monitoring, gain flattening of EDFAs, polarisation discrimination, and optical sensor interrogation [8].

In recent years, with the advancement in UV-inscription technology and the drive from the various new fibres, a variety of in-fibre gratings have been investigated and developed,

generating many smart device functionalities for applications in chemical detection, biosensing, bioengineering, environmental monitoring, medical science and health care.

This chapter is constructed as follows. In section 2, we give an overview of the optical fibre grating theories, including the mode coupling mechanism and phase matching condition. In Section 3, we present the fibre grating fabrication techniques. In section 4, we demonstrate several grating based optical fibre sensors for chemical and biosensing. Finally, a conclusion ends this chapter.

2. Theory of the optical fibre gratings

2.1. Coupled-mode theory

The coupled-mode theory is a basic theory for obtaining quantitative information about the diffraction efficiency and spectral dependence of optical fibre gratings. The derivation of the coupled-mode theory will not be provided, as it was detailed by Yariv and Kogelnik [1, 9]. Here the coupled-mode theory is briefly discussed following the work by Erdogan [3, 10].

The transverse component of the electric field in the ideal-mode approximation to coupled-mode theory can be written as a superposition of the ideal modes where the modes are in an ideal waveguide with no grating perturbation

$$\vec{E}_t(x,y,z) = \sum_j \left[A_j(z)\exp(i\beta_j z) + B_j(z)\exp(-i\beta_j z) \right] \cdot \vec{e}_{jt}(x,y) \tag{1}$$

where the coefficients $A_j(z)$ and $B_j(z)$ are the slowly varying amplitudes of the *j*th mode traveling in the +z and -z directions, respectively. $\vec{e}_{jt}(x, y)$is the transverse mode field, which might describe a bound-core, cladding or radiation mode. The propagation constant β is simply

$$\beta = \frac{2\pi}{\lambda} n_{eff} \tag{2}$$

Where n_{eff} is effective index of *j*th mode. The presence of a dielectric perturbation will cause the coupling between the modes. The amplitudes $A_j(z)$ and $B_j(z)$ of the *j*th mode then evolve along the z direction according to

$$\frac{dA_j(z)}{dz} = i\sum_k A_k(K_{kj}^t + K_{kj}^z)\exp[i(\beta_k - \beta_j)z] + i\sum_k B_k(K_{kj}^t - K_{kj}^z)\exp[-i(\beta_k + \beta_j)z] \tag{3}$$

$$\frac{dB_j(z)}{dz} = -i\sum_k A_k(K_{kj}^t - K_{kj}^z)\exp[i(\beta_k + \beta_j)z] - i\sum_k B_k(K_{kj}^t + K_{kj}^z)\exp[-i(\beta_k - \beta_j)z] \tag{4}$$

The transverse coupling coefficient between *j* and *k* modes in the above equations is

$$K_{kj}^{t}(z) = \frac{\omega}{4}\iint_{\infty}\left[\Delta\varepsilon(x,y,z)\vec{e}_{k}^{t}(x,y)\cdot\vec{e}_{j}^{t*}(x,y)\right]dxdy \tag{5}$$

The longitudinal coefficient $K_{kj}^{z}(z)$ is analogous to $K_{kj}^{t}(z)$, but for fibre modes $K_{kj}^{z}(z)$ is usually neglected since $K_{kj}^{z}(z) << K_{kj}^{t}(z)$. In (5), Δε(x, y, z) is the permittivity perturbation, for $\delta n_{eff} << n_{eff}$, which is approximately

$$\Delta\varepsilon(x,y,z) = 2n_{eff}\delta n_{eff}(x,y,z) \tag{6}$$

In an ideal waveguide situation where no perturbation exists (Δε=0), the coupling coefficient $K_{kj}^{t}(z)=0$, then the transverse modes are orthogonal and do not exchange energy.

Exposing photosensitive fibre to a spatially varying pattern of UV-light produces the refractive index change $\delta n_{eff}(z)$

$$\delta n_{eff}(z) = \overline{\delta n}_{eff}(z)\left[1+\upsilon\cos\left(\frac{2\pi}{\Lambda}z+\varphi(z)\right)\right] \tag{7}$$

where υ is the fringe visibility of the index change, Λ is the grating period, Φ(z) describes the grating chirp, and $\overline{\delta n}_{eff}(z)$ is the "dc" index change spatially averaged over a grating period, or the slowly varying envelope of the grating.

In most fibre gratings the UV-induced index change $\delta n_{eff}(x, y, z)$ is approximately uniform across the core and nonexistent outside the core. Thus the core index change can be described by an expression similar to (7) with $\overline{\delta n}_{eff}(z)$ replaced by $\overline{\delta n}_{co}(z)$.

Thus, with (6) and (7), the general coupling coefficient (5) may now be written

$$K_{kj}^{t}(z) = \sigma_{kj}(z) + 2\kappa_{kj}(z)\cos\left[\frac{2\pi}{\Lambda}z+\varphi(z)\right] \tag{8}$$

where δ is defined as a "dc" coupling coefficient and κ is an "ac" coupling coefficient

$$\sigma_{kj}(z) = \frac{\omega n_{eff}\overline{\delta n}_{eff}(z)}{2}\iint_{core}\vec{e}_{k}^{t}(x,y)\cdot\vec{e}_{j}^{t*}(x,y)dxdy \tag{9}$$

$$\kappa_{kj}(z) = \frac{\upsilon}{2}\sigma_{kj}(z) \tag{10}$$

2.1.1. Backward mode coupling

For the backward mode coupling, the dominant interaction is near the wavelength for which reflection occurs from a mode of amplitude $A(z)$ to an identical counter-propagating mode of amplitude $B(z)$. Under such conditions (3) and (4) can be simplified to the following equations [3]

$$\frac{dR}{dz} = i\hat{\sigma}R(z) + i\kappa S(z) \tag{11}$$

$$\frac{dS}{dz} = -i\hat{\sigma}S(z) - i\kappa^{*}R(z) \tag{12}$$

where the amplitudes R and S are

$$R(z) = A(z)\exp\left(i\delta z - \frac{\varphi(z)}{2}\right) \tag{13}$$

$$S(z) = B(z)\exp\left(-i\delta z + \frac{\varphi(z)}{2}\right) \tag{14}$$

In equations (11) and (12), κ is the "ac" coupling coefficient and $\hat{\sigma}$ is the general "dc" self-coupling coefficient defined as

$$\hat{\sigma} = \delta + \sigma - \frac{1}{2}\frac{d\varphi(z)}{dz} \tag{15}$$

with δ being the detuning, which is independent of z and is defined to be

$$\delta = \beta - \frac{\pi}{\Lambda} = \beta - \beta_d = 2\pi n_{eff}\left[\frac{1}{\lambda} - \frac{1}{\lambda_d}\right] \tag{16}$$

here $\lambda_d = 2n_{eff}\Lambda$ is the "design wavelength" for Bragg scattering by an infinitesimally weak grating ($\delta n_{eff} \to 0$).

For a single-mode Bragg grating, there are the following simplified relations

$$\sigma = \frac{2\pi}{\lambda}\overline{\delta n_{eff}} \tag{17}$$

$$\kappa = \kappa^* = \frac{\pi}{\lambda}\upsilon\overline{\delta n_{eff}} \tag{18}$$

If the grating is uniform along z direction, then $\overline{\delta n}_{eff}$ is constant and $d\varphi(z)/dz = 0$ which means no grating chirp. Thus κ, σ, and $\hat{\sigma}$ are constants. This simplifies (11) and (12) into coupled first-order ordinary differential equations with constant coefficients. The closed-form solutions may be found when appropriate boundary conditions are specified.

2.1.2. Forward mode coupling

For the forward mode coupling, close to the wavelength for which a forward- propagating mode of amplitude $A_1(z)$ is strongly coupled into a co-propagating mode with amplitude $A_2(z)$, (3) and (4) may be modified by retaining the terms that involve the amplitudes of these two modes and making the usual synchronous approximation

$$\frac{dR}{dz} = i\hat{\sigma}R(z) + i\kappa S(z) \tag{19}$$

$$\frac{dS}{dz} = -i\hat{\sigma}S(z) + i\kappa^* R(z) \tag{20}$$

where the new amplitudes R and S are

$$R(z) = A_1 \exp\left[-i(\sigma_{11} + \sigma_{22})\frac{z}{2}\right]\exp(i\delta z - \frac{\varphi}{2}) \tag{21}$$

$$S(z) = A_2 \exp\left[-i(\sigma_{11} + \sigma_{22})\frac{z}{2}\right]\exp(-i\delta z + \frac{\varphi}{2}) \tag{22}$$

In above equations, σ_{11} and σ_{22} are "dc" coupling coefficients defined in (9), $\kappa = \kappa_{21} = \kappa_{12}^*$ is the "ac" cross-coupling coefficient from (10) and $\hat{\sigma}$ is a general "dc" self-coupling coefficient now defined as

$$\hat{\sigma} = \delta + \frac{\sigma_{11} - \sigma_{22}}{2} - \frac{1}{2}\frac{d\varphi}{dz} \tag{23}$$

When the detuning δ is assumed to be constant along the z axis, it becomes

$$\delta = \frac{1}{2}(\beta_1 - \beta_2) - \frac{\pi}{\Lambda} = \pi\Delta n_{eff}\left[\frac{1}{\lambda} - \frac{1}{\lambda_d}\right] \tag{24}$$

where again $\lambda_d = \Delta n_{eff}\Lambda$ is the "design wavelength" for a grating approaching zero index modulation. In the case of Bragg gratings, $\delta = 0$, or $\lambda = \lambda_d = \Delta n_{eff}\Lambda$, corresponds to the grating condition.

For a uniform forward-coupled grating, $\hat{\sigma}$ and κ are constants. In contrast to the single-mode Bragg grating, here the coupling coefficient κ generally may not be written simply as in (18) and must be evaluated numerically. As the case of the FBG, the forward-coupled grating equations (19) and (20) are coupled first-order ordinary differential equations with constant coefficients. Thus when the appropriate boundary conditions are given, the closed form solutions can be found.

2.2. Phase-matching condition

If the perturbation exists in the fibre, the bound-wave can be coupled to the counter-propagating or co-propagating modes. Based on the direction of the mode coupling, fibre gratings may be classified in two types. One type is a backward-coupled grating which couples light to opposite directions. FBGs of normal and small-tilt uniform and chirped structures belong to this type. The other category is a forward-coupled grating, represented by LPGs and FBGs with largely tilted structures, where coupling occurs between the same directional modes.

For the coupled modes, the phase mismatch factor $\Delta\beta$ is referred as a detuning

$$\Delta\beta = \beta_i \pm \beta_d - \frac{2\pi}{\Lambda_g} N\cos\theta \tag{25}$$

where β_I and β_d are the propagation constants for the incident and diffracted modes, respectively, Λ_g is the period of the grating, θ is the grating tilt angle and N represents an integer number. It is noteworthy that the " $\pm$ " sign describes the case wherein the mode propagates in the $\mp$ z direction.

When the phase-matching condition satisfied $\Delta\beta$=0, (25) becomes

http://dx.doi.org/10.5772/54242

$$\beta_i \pm \beta_d = \frac{2\pi}{\Lambda_g}\cos\theta \tag{26}$$

If both β_1 and β_d have identical signs, then the phase will be matched for counter- propagating modes; if they have opposite signs, then the interaction is between co-propagating modes. In most cases, first-order diffraction is dominant, hence N is assumed to be unity [1].

The resonant wavelength should be satisfied

$$\lambda = (n_i^{eff} \pm n_d^{eff})\frac{\Lambda_g}{\cos\theta} \tag{27}$$

2.2.1. Fibre Bragg gratings

In the case of backward-coupling (Fig. 1), represented by normal FBG (θ=0°), the Bragg wavelength of the core mode is given by

$$\lambda_B = 2n_{eff}\Lambda \tag{28}$$

where n_{eff} is the effective index of the core.

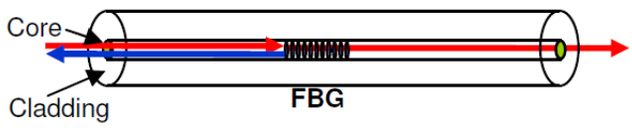

Figure 1. Schematic of a contradirectional mode coupling for FBG.

2.2.2. Long-period gratings

In the case of forward-coupling, represented by LPG (Fig. 2), the resonant wavelength for coupling between the core and cladding modes satisfy

$$\lambda_{res} = (n_{co}^{eff} - n_{cl,m}^{eff}) \cdot \Lambda \tag{29}$$

where n_{co}^{eff} and $n_{cl,m}^{eff}$ are the effective indices of the core and the mth cladding mode, respectively.

The differences between core and cladding mode effective indices are much smaller than unity, hence the grating period for a forward-coupled grating at a given wavelength is much larger

than that of a backward-coupled grating. Typically, LPG periods are hundreds of microns, whereas the period of FBG is less than a micron [11, 12].

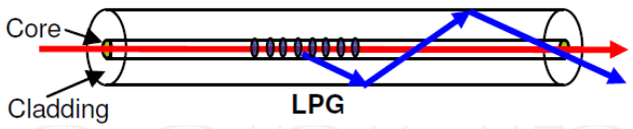

Figure 2. Schematic of a codirectional mode coupling for an LPG.

2.2.3. Tilted fibre gratings

In the case of tilted gratings, as shown in Fig. 3, the mode coupling becomes more complex. The resonant wavelengths are [8, 13]

$$\lambda_{co-cl} = (n_{co}^{eff} \pm n_{cl,m}^{eff}) \cdot \frac{\Lambda_g}{\cos\theta} \tag{30}$$

where n_{co}^{eff} and $n_{cl,m}^{eff}$, respectively, are the effective indices of core and the mth cladding mode. The grating period along the fibre axis is simply

$$\Lambda = \frac{\Lambda_g}{\cos\theta} \tag{31}$$

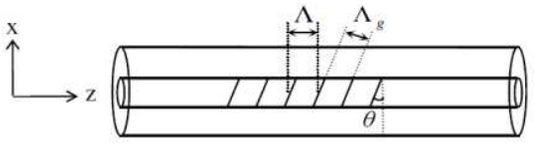

Figure 3. Schematic diagram of tilted grating in fibre core.

In equation (30), the sign of "+" and "-" describe the case wherein the mode propagates in -z or +z direction, relating to the grating tilt angle θ and then the backward- and forward- coupled TFG, respectively.

Mode coupling in a TFG can be understood by analysis of the phase-matching conditions as shown in Fig. 4(a). The strongest coupling takes place at the phase-matching condition

$$\vec{K}_R = \vec{K}_{co} + \vec{K}_G \tag{32}$$

http://dx.doi.org/10.5772/54242

where $\vec{K}_R$, $\vec{K}_{co}$ and $\vec{K}_G$ are wave vectors of the radiated light, core mode and grating itself, respectively. Because the refractive indices of the core and the cladding are very close, in general we may neglect the amplitude difference between $\vec{K}_R$and $\vec{K}_{co}$.

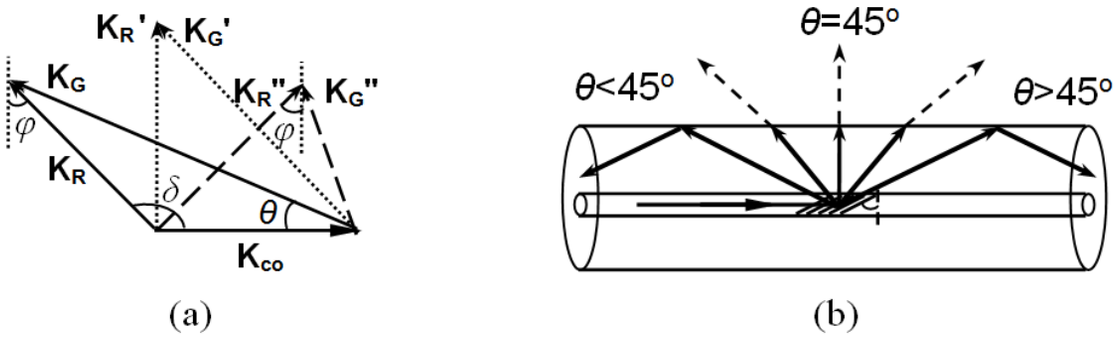

Figure 4. (a) Phase-matching conditions. (b) Mode coupling regimes for TFGs with tilt angles θ <, =, and >45°.

The direction of the coupled light depends on the tilt angle of the grating structure. As shown in Fig. 4(b), if the grating's tilt angle θ <45° (i.e. the radiation angle δ is an obtuse angle), the core mode will be coupled to the backward-propagating direction; if the grating angle θ>45° (δ is an acute angle), the core light can be coupled to the forward-propagating direction; if the θ=45° (δ=90°), all the phase matched light will be completely radiated out of the fibre. However, due to the total internal reflection effect at the cladding boundary, the coupled light by the TFG will exist in two different ranges: in one case the light radiated out of the core will be confined and propagates in the cladding; in the other case the light will not be bound by the cladding and will be tapped out from the side of the fibre. The range for radiation mode coupling depends on the critical angle, which is defined as

$$\alpha_c = \arcsin\frac{n_1}{n_2} \tag{33}$$

where n_1 and n_2 are refractive indices of the surrounding-medium and cladding, respectively. If the fibre is surrounded by air (n_1~1.0), the critical angle α_c=43.8°. If the surrounding-medium changes to the water (n_1~1.33), the critical angle α_c=67.0°.

If we define the incident angle as φ, shown in Fig. 4(a), for the light phase matched and radiated out of the core to the cladding /surrounding-medium boundary, φ is related to the grating tilt angle θ by φ=|2θ-π/2|. If $\varphi < \alpha_c$, the radiation mode coupling range will be given by $\theta_{1c} < \theta < \theta_{2c}$ can be calculated as

$$\theta_{1c} = \frac{1}{2}\left(\frac{\pi}{2} - \alpha_c\right) \qquad \theta_{2c} = \frac{1}{2}\left(\frac{\pi}{2} + \alpha_c\right) \tag{34}$$

We have calculated this range to be 23.1°~66.9° in air and 11.5°~78.5° in water surrounding-medium. Within this range, the light will not be confined by the cladding and will radiate from the fibre. Below or beyond this range, the light will be coupled to the backward- or forward-propagating cladding modes, respectively, and be bound within the fibre.

3. Grating fabrication techniques

The fibre grating fabrication techniques may be classified to three main categories: two-beam holographic, phase mask and point-by-point techniques. Each technique has its merits and limitations and will be employed according to the specification requirement of the gratings to be fabricated.

3.1. Two-beam holographic technique

Fig. 5 shows the two-beam holographic UV-inscription system. The UV-beam is split into two with equivalent power when it passes through a 50:50 beam splitter. The two beams are then reflected by highly reflective mirrors M_1 and M_2 to meet on to the same section of the photo-sensitive fibre to produce the interfering fringes. A beam expanding telescope system consisting of two cylindrical lenses (C and D), where $df=CD-(f_c+f_d)=0$, is inserted into the optical path to expand the width of UV Gaussian beam, and thus the length of the two-beam interference pattern on the forthcoming meet at point O. Two cylindrical lenses (F_1 and F_2) are employed to focus the beams to the fibre core with enhanced power intensity.

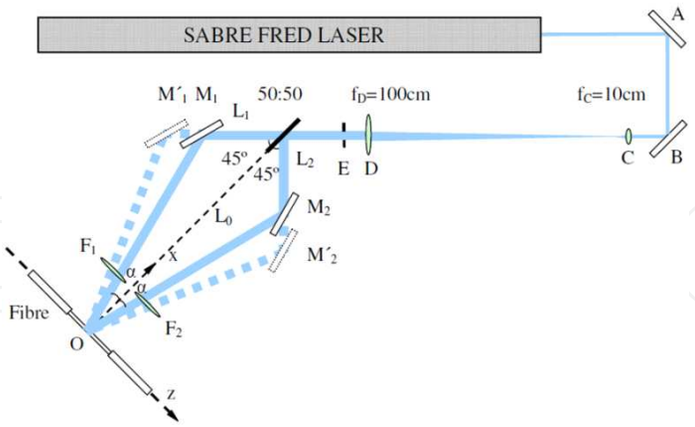

Figure 5. Two-beam holographic FBG inscription system.

The major advantage of the two-beam holographic method is the ability to write gratings with arbitrarily selected wavelengths simply by adjusting the angle (2α) between the two beams [14]. Limited by the range of the optical spectrum analyser (OSA) and the light source, the gratings fabricated are normally in the range of 750nm to 2000nm.

3.2. Phase-mask technique

The phase-mask technique, based on near-contact UV-beam scanning a phase mask, is one of the most effective techniques for reproducible FBG inscription.

The grating written by phase mask technique has a period of

$$\Lambda = \frac{\lambda_{UV}}{2\sin\theta_m} = \frac{\Lambda_{PM}}{2} \tag{35}$$

where Λ_{PM} is the period of the phase mask. The Bragg wavelength is then given by [3]

$$\lambda_B = 2n_{eff}\Lambda = n_{eff}\Lambda_{PM} \tag{36}$$

The phase mask is a corrugated grating etched in a silica substrate produced by high resolution lithography. Important features in a phase mask are the period of the etched grooves and the etch depth. With normal incidence, the UV-radiation is diffracted into several orders, m=0, ±1, ±2… The commercial phase masks have been optimized to achieve 0-order suppression of <5% and ~40% transmission in each of the ±1 diffracted orders. The superposition of ±1 diffraction orders, in the proximity of the surface of the phase mask, produces an interference pattern that can be used for writing FBGs.

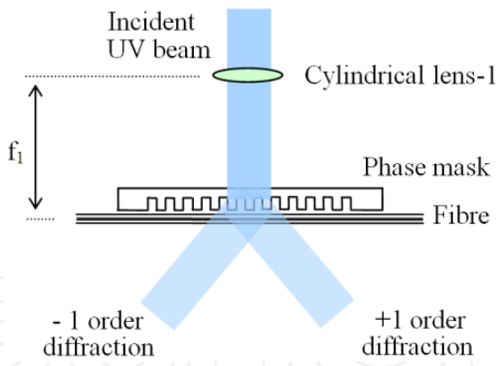

Figure 6. Fibre grating inscription by UV-beam scanning across a phase mask.

As shown in Fig. 6, a cylindrical lens with a focal length f_1 is added before phase mask and focuses the UV-irradiation to the fibre core with increased intensity in one dimension in the beam-fibre plane. Very uniform index modulation can be achieved by the phase mask method. Fig. 7(a) shows the image of the fringe structure inscribed in the fibre core using the phase mask method. The image was examined and measured by use of the Axioskop2 mot plus microscope (Carl Zeiss) in conjunction with Axio vision Cameras &Framegrabbers system with high magnification. Fig. 7(b) shows the typical transmission spectra for a uniform FBG fabricated by the phase mask technique. The grating is 5mm long and is designed to reflect

with a Bragg wavelength of 1550nm. The multiple resonances with smaller amplitude on the short wavelength side of the main Bragg resonance are due to the radiated mode being reflected at the cladding-air interface and re-entering the core, creating a cylindrical Fabry-Perot effect.

Besides the distinctive advantage of reproducible grating inscription, a further advantage of the phase-mask technique is the ability to make high quality, complex grating structures, including grating arrays, chirped [15-17], apodised [18, 19], phase-shifted [20, 21], Moire [22, 23], sampled [24], and long-length gratings [25]. Of particular relevance to the work presented in this chapter, the phase-mask method has also been employed to fabricate TFGs with tilted structures ranging from 0° to 84°. In the phase mask fabrication system, TFGs can be realised simply by rotating the phase mask with respect to the fibre. Chirped gratings can also been readily fabricated using a chirped phase mask in this system.

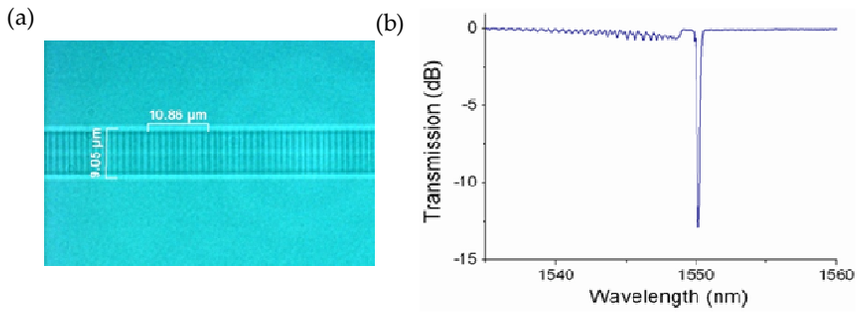

Figure 7. (a) Image of an FBG written by phase mask method (b) The typical transmission profiles of an FBG.

A disadvantage of the phase mask method is the limit to variation of Bragg wavelength, as it needs a separate phase mask for different wavelength required. The strain-fibre method has been incorporated into the system to give a 2nm-tuning range to the Bragg wavelength for each mask.

3.3. Point-by-point technique

The third main grating fabrication technique is the point-by-point technique. Because the grating is written a point at a time, it is a flexible method to alter the grating parameters, such as length, periodicity and strength. Limited by the focused spot size of UV-beam, it is difficult to control translation stage movement accurately enough to write FBG structures which in general have typical periods of ~0.5μm at 1550nm. Thus, the point-by-point technique is mainly used to fabricate long-period gratings with periods ranging from 10μm to 600μm.

As shown in Fig. 8(a), the point-by-point inscription system, two cylindrical lenses are added to focus the writing beam on the fibre to an approximate spot size of 20μm×20μm in z- and y-dimension and a shutter is computer- programmed to switch on/off with a 50:50 duty cycle to realise period-by-period print. The system has a great flexibility in fabricating LPGs with different periods, lengths and strengths. Fig. 8(b) shows the typical transmission spectrum of an LPG in SMF-28 with a length of 40mm and a periodicity of 380μm made by the point-by-

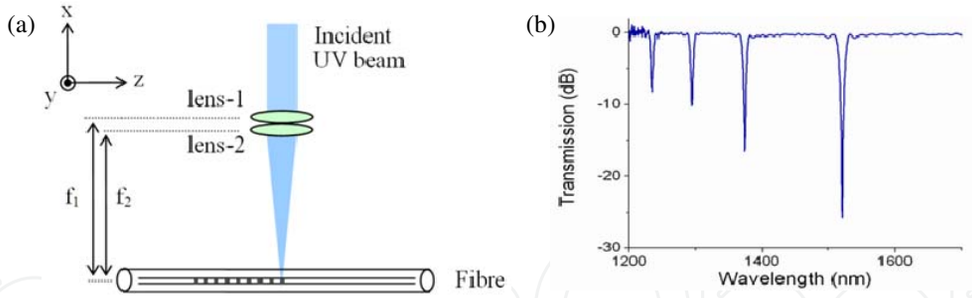

Figure 8. (a) Schematic of LPG fabrication using point-by-point technique. (b) The typical transmission spectrum of an LPG in SMF-28 fibre.

point method. The four broad attenuation resonances within 1200~1700nm wavelength range correspond to coupling to the different cladding modes. The bandwidth of resonances of an LPG is typically >10nm, much broader than that of an FBG. LPGs are transmission loss type devices and have been employed for a range of applications in optical communications and sensing.

3.4. Inscription of tilted fibre gratings

FBGs with tilted structures have their unique device functionalities. This section will present the fabrication and spectral characterisation of TFGs.

3.4.1. Design principle of TFGs

As illustrated in Fig. 9 the tilted structures can be achieved either (a) by tilting the phase mask with respect to the fibre in the phase mask inscription system, or (b) by rotation of the fibre about the axis normal to the plane defined by the two interfering UV beams in the holographic system.

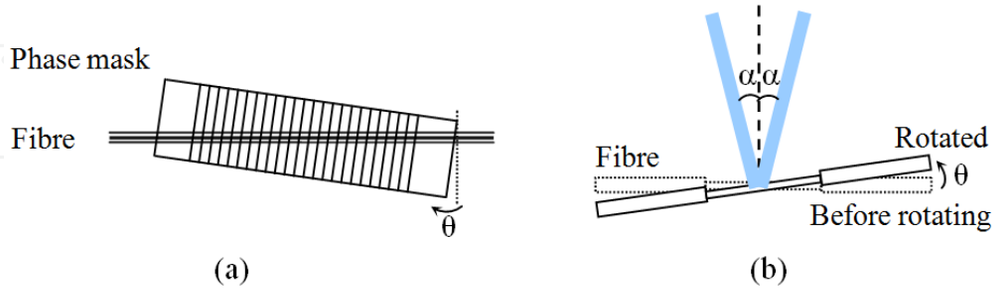

Figure 9. (a) Phase mask and (b) two-beam holographic techniques for TFG fabrication.

Owing to the cylindrical geometry of the optical fibre, the internal grating angle θ_{int} is not the same as the external phase-mask angle or fibre rotated angle θ_{ext}. For the phase-mask fabrication, the internalgrating angle θ_{int} is related to the external phase mask tilt angle θ_{ext}(the angle between the mask and the fibre) by the following relationship [26]

$$\theta_{\text{int}} = \frac{\pi}{2} - \tan^{-1}\left[\frac{1}{n\tan\theta_{ext}}\right] \tag{37}$$

In the case of holographic fabrication, θ_{int} can be expressed as [8]

$$\theta_{\text{int}} = \frac{1}{2}\left[\arcsin\left(\frac{1}{n}\sin(\alpha+\theta_{ext})\right) - \arcsin\left(\frac{1}{n}\sin(\alpha-\theta_{ext})\right)\right] \tag{38}$$

where α is the half angle between the two interfering beams, θ_{ext} is the fibre tilt angle.

The comparative study on TFG inscribed by phase mask and holographic method has been reported in [27], here we main focus on the phase mask fabrication of TFGs. The relationship of external and internal tilt angles for TFGs written by phase mask method has been depicted in Fig. 10.

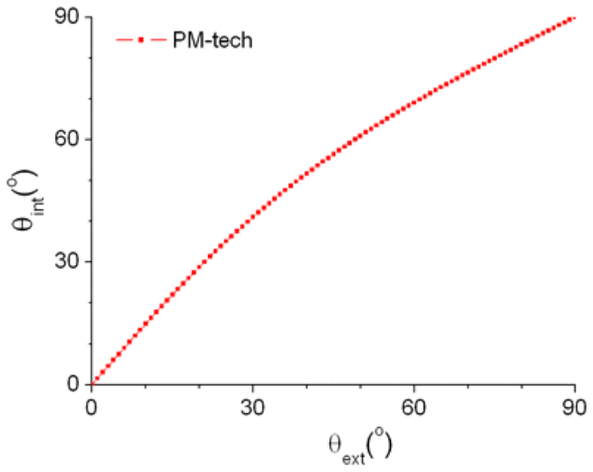

Figure 10. The relationship of the internal angle θ_{int} against the external angle θ_{ext} for TFG.

3.4.2. Unique spectral characteristics of TFGs

One of the unique characteristics of TFGs is the strong polarisation dependent loss (PDL) effect when the tilt angle becomes large. This property has been implemented as an in-line polarimeter [28] and a PDL equaliser [29, 30]. In addition, a near-ideal in-fibre polariser based on 45°-TFG has been reported by [31, 32], exhibiting a polarisation-extinction ratio higher than 33dB over 100nm range and an achievement of 99.5% degree of polarisation for the unpolarised light.

It is well known that there are two components of the electric field vector in the plane of polarisation. The components of the electric field parallel and perpendicular to the incidence plane are termed p-like and s-like. Light with a p-like electric field is defined to be p-polarised

http://dx.doi.org/10.5772/54242

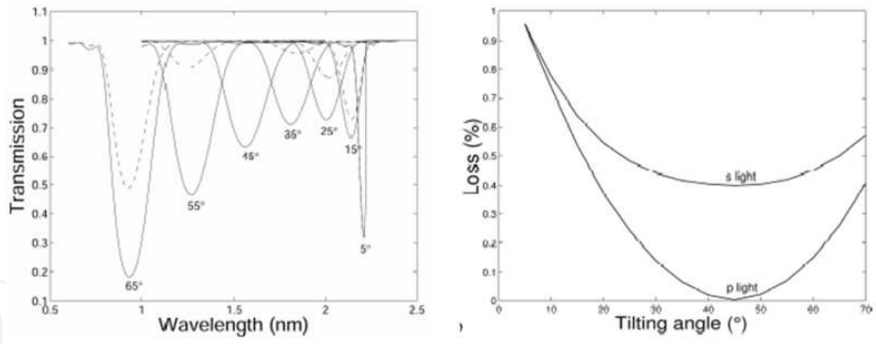

Figure 11. (a) The simulated transmission spectra of p- (dashed line) and s-polarised mode (solid line) travelling in the TFGs with various tilting angles; (b) Transmission losses of s- and p-polarised mode versus tilting angles. (After: [32])

whereas light with an s-like electric field is s-polarised. Fig. 11(a) shows the simulated transmission profiles of both the s- and p- polarised modes after they pass through a TFG. It is clear that both of two polarised modes show similarly evolving trends although the change in amplitude for p-polarised mode is more noticeable. The maximum transmission losses for different tilt angles for s- and p- modes have been simulated and plotted in Fig. 11(b). The transmission loss reaches minimum when the tilt angle is at 45°. At this critical angle, the loss of p-mode is eliminated completely and s-mode loss is still noticeably high [32], ie. p-mode is transmitted and s-mode is completely attenuated.

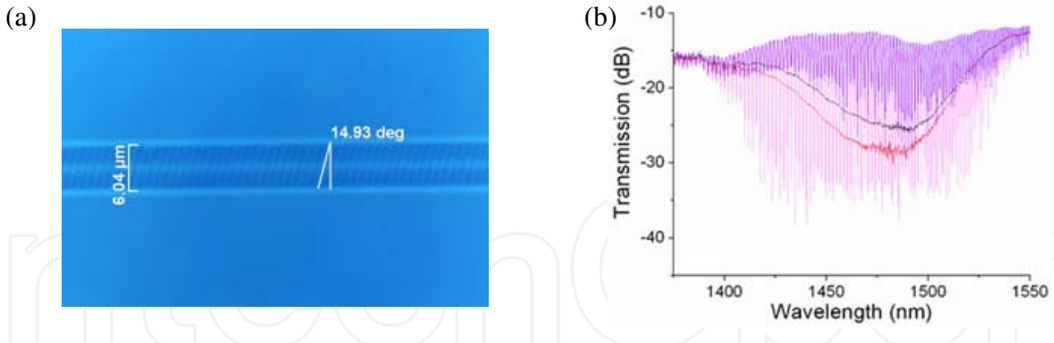

Figure 12. Image of 10°$_{ext}$-TFG in B/Ge fibre (a) and transmission spectra (b).

As an example, a photo-induced tilted index modulation is shown in Fig. 12(a). This is θ_{ext}=10° tilted grating, the measured internal angle θ_{int} is 14.93° which is in a good agreement with the theoretical result (θ_{int}=14.9°) from Equation (37). Fig. 12(b) plots its transmission spectra where the dense resonances covering 1375-1550nm are caused by the core-cladding coupling and by the reflection at the cladding-air boundary. The multiple resonances can be removed by immersing the grating in index-matching gel to simulate an infinite cladding, where the light

is coupled from the core to radiation modes, thus the dense resonances evolve to a smooth transmission loss profile.

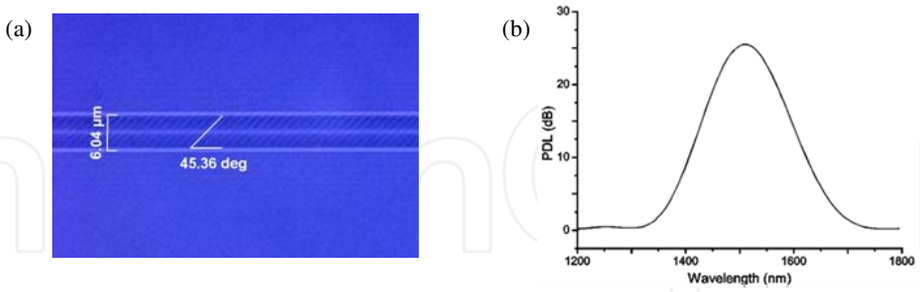

Figure 13. Image of 45°-TFG (a) and its PDL profile (b).

An 45°-TFG was fabricated in Ge-doped photosensitive fibre using the scanning phase mask technique and 244-nm cw UV laser source. A phase mask with 1.8μm period was used to ensure the 45°-TFG spectral response fell into near 1550nm region, the phase mask was rotated by 33.3° to induce slanted fringes at 45° within the fibre core. The 45° tilted fringes, shown in Fig. 13(a), were verified by examination with an oil-immersion high-magnification microscope. Fig. 13(b) shows the PDL of a 25mm-length 45°-TFG, the entire PDL profile is near-Gaussian-like distribution over ~300nm with the maximum PDL of 26dB at 1520nm [33].

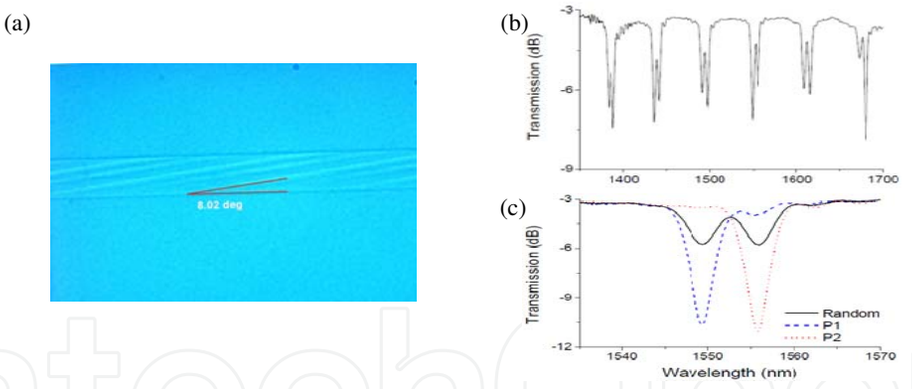

Figure 14. Image of the 81°-TFG (a) and it transmission spectra (b-c).

We fabricated a 10mm long 81°-TFBG in SMF-28 with UV laser scanning the phase mask (with period of 6.6μm) method. Fig. 14. (a) shows the image of the tilted fringes with a measured internal angle of 81.98°.

Since the angle 81° $>\theta_{2c}$ (=66.9° in the air), the light was coupled to forward-propagating cladding modes corresponding a series of the resonances with a noticeable paired-peak feature on the spectra, Fig. 14(b), it may be expected that the highly tilted structures will increase the birefringence of the fibre, thus resulting in the light coupled to two sets of modes of different polarisation states. It can be noticed that the strengths of the paired-peaks in Fig. 14(b) are around 3dB, which suggests that the light may be coupled equally into two sets of birefringence

http://dx.doi.org/10.5772/54242

modes corresponding to the two orthogonal polarisation states. To confirm this, a polariser and a polarisation controller were inserted in the measurement system to measure the transmission spectrum. By varying the polarisation state of the probe light, the strengths of the paired-peaks varied accordingly with the polarisation of the light. Fig. 14(c) shows the transmission spectra of one of the paired-peak around 1550nm for random and two orthogonally polarised states. With random polarisation, both peaks exhibit a ~3dB loss as the light is coupled equally to the birefringence modes. When the light is switched to either polarisation state, one resonance grows into its full strength ~7.3dB whereas the other almost disappears. The polarisation effect induced spectral separation between the paired-peaks is about 6.3nm, giving an estimated birefringence of ~10^{-4}.

4. Optical fibre grating based chemical and bio- sensors

A key characteristic of optical chemical and bio- sensor design is the sensitivity to, or the change rate of optical signal as a function of, surrounding chemical and bio- analyte. There has also been an increasing activity aimed at implementing optical biosensors by exploring the fibre grating's response to the change of surrounding-medium refractive index (SRI) [34, 35, 36-38].SRI-sensitive devices have been recently developed by UV-inscribing normal Bragg, tilted, and long-period structures in standard single, multimode, and D-fibres[39-43]. Appropriate choice of fibre type can provide intrinsic or enhanced SRI sensitivity to grating structures and allow, in some instances, the realisation of multifunctionality. The fibre grating based RI sensors can be coated with bioactive materials to interact with certain type of biological agents, thus become true biosensors with high sensitivity and selectivity [44, 45].

4.1. Refractive index sensing principle of in-fibre gratings

As a core-to-core mode coupling, the light in an FBG is well screened by the cladding, effectively precluding strong interaction with the surrounding medium. Thus it is intrinsically insensitive to SRI. Several techniques have been demonstrated to sensitise FBGs, including polishing and chemical etching the fibres to expose the core to surrounding medium.

In contrast to FBGs, LPGs, as core-cladding mode coupling devices, are intrinsically sensitive to SRI. Any variation in the core-cladding guiding properties will affect the transmission characteristics of LPGs, providing an optical signal encoded with the information of external parameters. LPGs have been used to monitor the physical parameters such as strain, temperature, load, curvature and with a variety structures for SRI sensing [35, 38].

4.2. Chemical etching technique for sensitisation

The chemical etching technique has been extensively employed to remove the claddings of the FBG structures, enabling the interaction of the core mode with the surrounding medium [46-48]. Although LPGs are intrinsically sensitive to SRI, modifying the cladding properties can further enhance their SRI sensitivity greatly. Chiang *et al*. reported the enhancement of the external refractive index sensitivity of an LPG resulting from a small reduction in the cladding

radius via an HF-etching process [49, 50]. We also employed the HF etching technique to reduce the thickness of the cladding of LPG devices and have demonstrated effective enhancement of the SRI sensitivity to these LPG structures.

In order to effectively control the thickness of the fibre gratings, an etching procedure was first established and the etching rates were investigated for different type fibres using HF acids of different concentrations. The HF etching technique inevitably suffers from mechanical reliability since any micro-crack of fibre will be very vulnerable to the HF acid, thus it will degrade the fibre tensile strength by orders of magnitude [51]. To effectively control the cladding size of fibre, the etching rate was first evaluated for virgin fibre samples including standard SMF and D-fibre using HF at 10% concentration. Twenty samples of each type fibre were immersed in the HF bath and were withdrawn in turn every 10min. The samples with differently etched claddings were then examined and measured by microscope with high magnification.

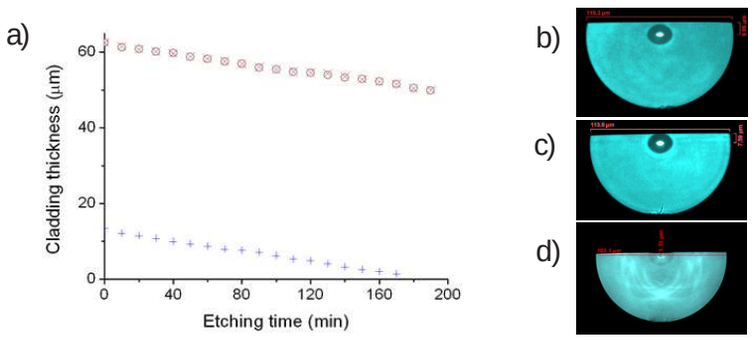

Figure 15. (a) Etching rates of SMF and D-fibre. (symbol × and o: round-side radii of SMF and D-fibre; symbol +: D-shaped cladding thickness of flat-side); The cross-section images of etched D-fibre: (b) etched-40min, (c) etched-90min, (c) etched-170min.

Fig. 15 plots the etched cladding thickness against etching time for the two types of fibre. The natural silica claddings of SMF and D-fibre show nearly isotropic etching processes with a similar etching rate of ~0.068μm/min. The cross-sectional images of the D-fibre samples that had been etched for 40min, 90min and 170min are shown in Fig. 15(b-d), respectively. It was estimated that at ~85min, the side of the inner elliptical fluorine-doped cladding on the flat side of the D-fibre was completely etched off, and the total inner cladding was almost removed after ~167min. After~170min, the core was almost etched off, as can be seen in Fig. 15(d), and the residual D-fibre cladding layer on the round-side was about 50.7μm.

Calibration of RI and sugar concentration

Since the chemical sensing mechanism of the in-fibre gratings is based on the resonances response to the change of SRI and the most devices discussed in this chapter have been evaluated for their SRI sensitivity by measuring the concentrations of sugar solution, the calibrated correlation between the concentration of sugar solution and the refractive index (RI) is necessary to be discussed first. Table 1 lists the conversion relationship between the percentage sugar concentration and the refractive index, which is from the data reported in reference [52].

Mass% of sugar solution	0	10	20	30	40	50	60	70	80
Refraction Index	1.333	1.348	1.364	1.381	1.400	1.420	1.442	1.465	1.491

Table 1. Calibration of refractive index against concentration of sugar solution ($C_{12}H_{22}O_{11}$).

4.3. Chemical sensor based on FBGs in D-fibre

In-fibre optical chemical sensor based on FBG in D-fibre and sensitised by HF etching treatment has been implemented and characterised.

The FBG structures were UV-inscribed in D-fibres using the standard phase mask fabrication method. The D-fibre FBG samples were then sensitised by removing the cladding layer on the flat side by employing etching process using HF acid of 10% concentration. In order to control the etching depth, the transmission spectra were monitored *in-situ* using an EDFA source and an optical spectrum analyser. Fig. 16 shows the spectral evolution of etched FBG samples the wavelength shift and strength of the transmission loss peak against etching time. There are three stages can be seen from the etching process: (i) 0~140min, (ii) 140~168min, and (iii) 168~173min. For the first stage, the spectrum of FBG remained intact, signifying the core mode was still well bounded by the cladding layer. With further etching (140~168min), the thickness of the flat-side claddingwas reduced to just a few microns, thereby allowing the evanescent field to penetrate to surrounding-medium (HF acid). In this stage, the Bragg resonance shifted noticeably towards the shorter wavelength side, indicating that the device has entered the SRI sensitive regime. For the final etching period from 168 to 173min, a fractional layer of the core was been etched off. As it can be seen from Fig. 16(b), the transmission loss drops dramatically due to the combined effects of the reduction of the effective core mode index and the degradation of the light confinement.

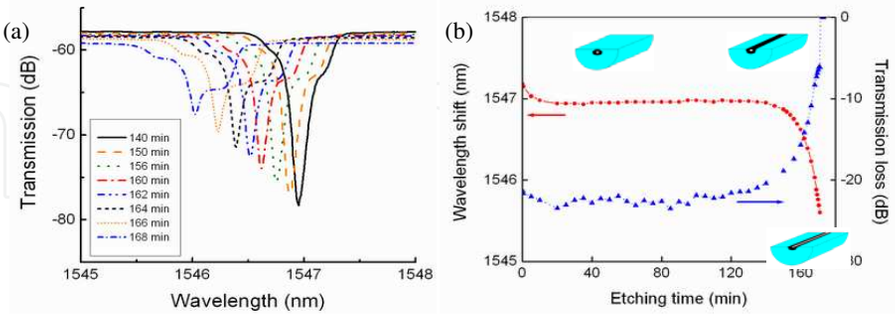

Figure 16. (a) Spectral evolution of the D-fibre FBG under etching period from 140~168min. (b) Bragg wavelength shift and transmission loss over the entire etching process. Inset, schematic images of D-fibre corresponding the different etching stage.

The SRI sensing characteristics of one un-etched and two etched D-fibre FBG devices (labeled as G1 and G2) were comparatively investigated. G1 and G2 were etched for 159min and 169min respectively. Sugar solutions with concentration ranging from 0% to 60% were prepared for

refractive index measurement. The three grating devices were immersed in turn into each sugar solution and their Bragg wavelengths were measured and are shown in Fig. 17 It is clearfrom this figure that the un-etched grating is totally insensitive to SRI whereas the Bragg wavelengths of G1 and G2 red-shift at different rates with increasing SRI. The deeper etched grating G2 exhibits a much higher SRI sensitivity than the less etched G1.

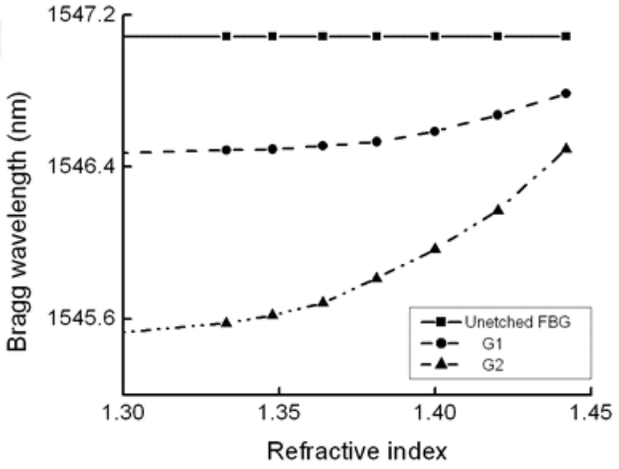

Figure 17. SRI sensitivity for un-etched, shallowly (G1) and deeply (G2) etched FBG in D-fibre.

If the SRI sensitivity is defined as the wavelength shift induced by 1% RI change, the maximum sensitivities exhibited by G1 and G2 are 0.03nm/% and 0.11nm/%, respectively. The latter is almost four times that of the former. Using the calibration of RI against sugar concentration, the SRI sensitivity can be converted to the sugar concentration sensitivity. For practical applications, up to 5% concentration change in sugar concentration can be easily detected by G2 using a standard optical interrogation system with an optical resolution of ~0.1nm and 0.5% change with a resolution of 0.01nm.

4.4. Dual-peak LPG for Haemoglobin sensing

In this section, an implementation of optical biosensor based on etched dual-peak LPG will be discussed. This device has been used to detect concentration of Haemoglobin (Hgb) protein in sugar solution, showing an ultrahigh sensitivity.

Due to the parabolic characteristic of the group index of the high-order cladding modes [34, 35], there exists a set of dispersion-turning-points on the LPG phase curves, where $d\lambda / d\Lambda \to \infty$. The nature of the coupled cladding modes close to the dispersion-turning-point makes the dual-peak LPGs ultrasensitive to cladding property, allowing fine tailoring the mode dispersion and index sensitivity by light-cladding-etching method using HF acid. It has been reported that the responses of such LPGs can be modified by reducing the cladding size via chemical etching [39, 41, 49, 50].

http://dx.doi.org/10.5772/54242

Based on the mode coupling theory, the phase curves have been simulated for an LPG of 160μm period in SMF-28 fibre with cladding radius reducing from 62.5μm to 51.5μm, as shown in Fig. 18(a). The dispersion-turning-point feature is apparentthat the slope direction of the phase curve changes from negative ($d\lambda / d\Lambda < 0$) to positive ($d\lambda / d\Lambda > 0$). For a given radius as dotted line in Fig. 18(a), two cladding modes, one in the positive and the other in negative dispersion region, could satisfy simultaneously the same phase match condition, resulting in dual-peak resonances.

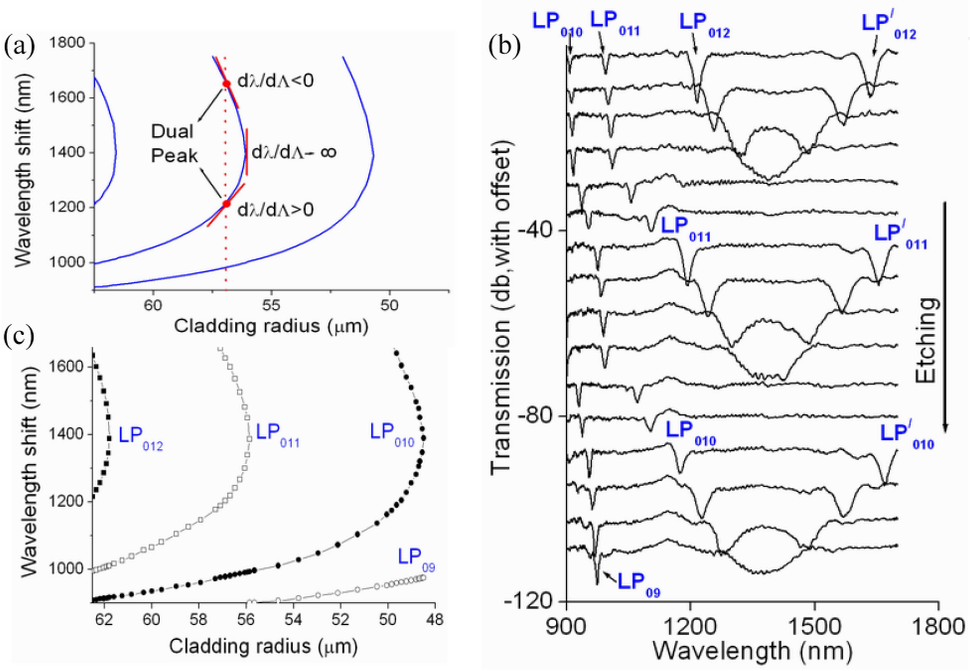

Figure 18. (a) Simulated phase curves of a dual-peak LPG of 160μm period for reduced cladding radius from 62.5μm to 51.5μm. (b) Spectral evolution of dual-peak LPG (c) Wavelength shift of LPG resonances against fibre cladding radius.

A dual-peak LPG with a period of 159μm was subjected to the etching experiment using an HF solution with 12% concentration. As the first trace shown in Fig. 18(b), this grating has four coupled cladding modes identified as LP_{010}, LP_{011}, LP_{012} and LP'_{012}in the wavelength range from 900nm to 1700nm, two of which are the dual-peak modes located at 1214.9nm and 1634.4nm. Under etching, it can be seen clearly that a transition of generation, coalescing and annihilation of the dual-peak resonances from higher order modes to lower ones. Firstly, LP_{012} and LP'_{012} are moving towards each other and eventually coalesced and annihilate, and a new pair of dual-peak modes (LP_{011} and LP'_{011}) are generated in conjunction with the red-shifting of LP_{010}; then this transition is repeated leading to the appearance of paired LP_{010} and LP'_{010}, and LP_{09} modes.

Fig. 18(c) plots the resonance shifts of dual-peak LPG against cladding radius, the shift speed increases when they are close to the dispersion-turning-point. It was also noticed that the movements of the same order dual peaks are not linear and symmetric: the loss peak with

longer wavelength in $d\lambda / d\Lambda < 0$ region moves faster than its counterpart at shorter wavelength in $d\lambda / d\Lambda > 0$ region.

When the dual-peak cladding modes are close to the dispersion-turning-point, it is possible to fine tuning the sensitivity by light etching the cladding. A light-etching experiment was performed using HF acid of only 1% concentration. A 20mm-long LPG with a 147μm period was subjected to etching for 96.5min, removing cladding thickness by only 1.1μm (from 62.5μm to 61.4μm). The spectral evolution was monitored for the etching process and plotted in Fig. 19(a). The dual peaks were originally at M and M′ spaced by 493.6nm and finally moved to N and N′ separated by only 98.1nm, indicating they are now much closer to the dispersion-turning-point and should be significantly more sensitive to SRI change.

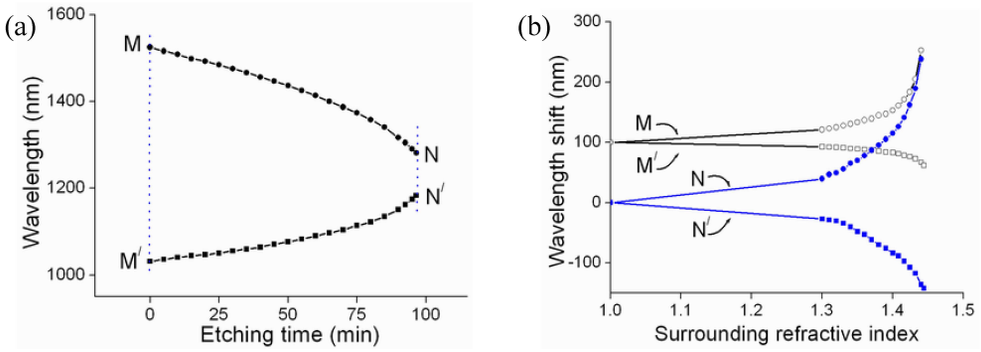

Figure 19. (a) Dual peak wavelengths against etching time (towards dispersion-tuning-point); (b) SRI induced spectral separation of the dual peaks for etched (N, N′) and unetched (M, M′) gratings (note: the curves have been offset).

The SRI sensitivity of the lightly etched dual-peak LPG was compared with that of an unetched device of the same grating parameters. The two gratings were immersed in the air and a set of index gels with refractive indices ranging from 1 to 1.44 and the separation of the dual peaks was measured for each SRI value, as plotted in Fig. 19(b). The separation increases nonlinearly with increasing SRI, however, that is far larger for the lightly-etched device than for the non-etched one. For SRI varying from 1 to 1.44, the total separation between N and N′ is 373.9nm, whereas that between M and M′ is 185.4nm, only half of the former. This indicates that the SRI sensitivity of the finely-etched LPG has more or less doubled that of the unetched one.

The lightly-etched dual-peak LPG was then used to measure the concentration of Hgb in sugar solution. Firstly, a set of Hgb solutions with concentrations from 0.0% to 1.0% (step 0.2%) was prepared by adding Hgbto water. Then 5ml each of these solutions was added into six beakers, each beaker had 30g of 60% aqueous sugar solution. LPG sensor was submerged in these solutions in turn and the shifts of 'N' peak were measured. Fig. 20(a) shows the spectral evolution the N-peak under different solutions and Fig. 20(b) plots its central wavelength shift against Hgb concentration. When the Hgb concentration changing from 0.0% to 1.0%, the peak red-shifts by 19.8nm. Defining the concentration sensitivity as the shift induced by 1% Hgb, we have a device sensitivity of ~20nm/1%. Thus, using a standard interrogation system with a resolution of 0.1nm, this finely tailored device could detect the Hgb concentration change as small as 0.005%.

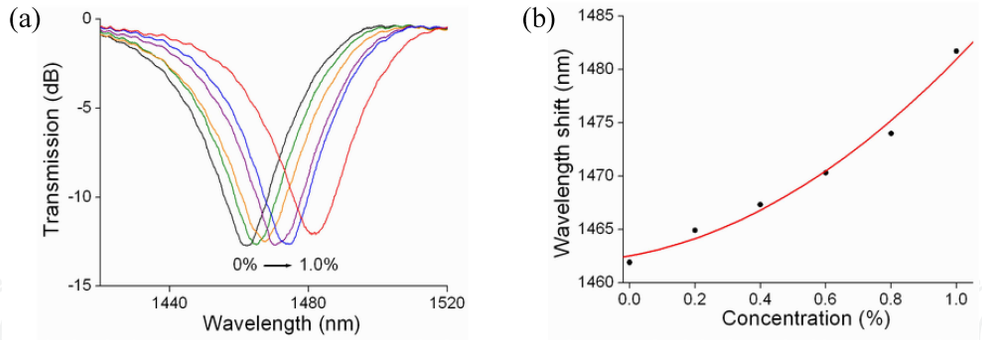

Figure 20. (a) Spectral evolution of N-peak of the lightly-etched dual-peak LPG with different Hgb concentrations; (b) N-peak wavelength shifts against Hgb concentration.

4.5. LPG based biosensor for DNA hybridisation detection

The development of biosensors is motivated by their potential applications in biochemical, biomedical, and environmental areas. In the past decade, the immobilisation techniques have been developed to enable the functionalisation of silica support and several DNA biosensors have been presented based on the hybridisation of target sequence to the bound DNA at the surface of modified electrode, surface plasmon resonance, microchips, ring-resonator, planar waveguide and optical fibre [53-55]. Chryssis*et al.* recently reported a detection of hybridisation of DNA by highly sensitive etched core FBG sensors [44, 45, 56-58]. Fibre grating based biochemical and biomedical sensors could be the alternative to and even the replacement for conventional biosensors with advantages, such as highly-sensitive, label-free, fast and real-time detection, dynamic analysis, etc. With the robustness and low-cost fabrication, the sensitised dual-peak LPGs could be another desirable candidate for advanced optical biosensors.

Here, we implement an optical biosensor based on LPG for detecting DNA interactions at a silica-liquid interface. The probe DNA is covalently immobilised onto the functionalised surface of the fibre grating region. Since LPG couples the light from core to cladding, it is intrinsically sensitive to changes in the refractive index at the sensor surface, thereby allowing the interaction between bound probe DNA and target DNA in ambient solution to be monitored *in situ*. This novel biosensor presents many advantages, such as detection of DNA hybridisation in low concentrations, real-time monitoring, high sensitivity and reusability.

Generation scheme of biosensor based on LPG: Fig. 21 displays the procedure of the in-fibre grating biosensor for silanisation, covalent activation, immobilisation and DNA hybridisation. All the biochemical experiments were performed in a fume cupboard. To minimise the bend cross-sensitivity, the LPG sensors were placed straight in a V-groove container on a Teflon plate and all the chemicals and solvents were added and withdrawn from the container by carefully pipetting.

Silanisation of LPG Surface: Prior to silanisation, LPGs were cleaned by immersion in 5M hydrochloric acid (HCl) for 30min at room temperature followed by rinsing in deionized (DI) water three times and drying in the air. Silanisation of glass surface was implemented by immersion in fresh 10% 3-Aminopropyl-triethoxysilane (APTS) (Sigma-Aldrich Company

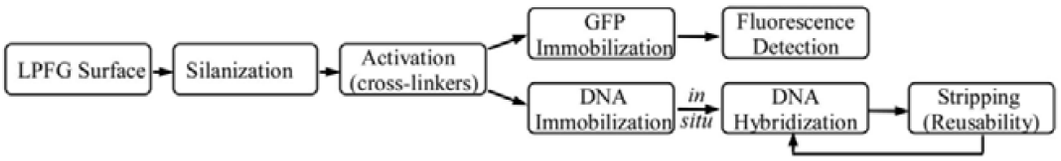

Figure 21. Basic scheme of the functionalisation of LPG for the generation of biosensor.

Ltd.) for 30min at room temperature [57]. In this work, a 30mm-long LPG with a period of 161μm has been used and the peak at 1590.5nm has been selected for biosensing experiment.

LPG Surface Activation: To immobilise biomolecules covalently to the glass surface, a chemical bond has to be formed between a functional group of biomolecule and the amino-group of the linker [54]. As it well known in bioconjugate chemistry, Dimethyl suberimidate (DMS, the molecular structure shown in Fig. 22(a)) is water soluble, membrane permeable and is one of the best crosslinking agents to convert the amino-groups into reactive imidoester cross-linkers. The imidoester functional group is one of the most specific acylating groups available for the modification of primary amines and has minimal cross reactivity toward other nucleophilic groups in proteins [59, 60]. In addition, DMS does not alter the overall charge of the protein, potentially retaining the native conformation and activity of the protein. For activation of glass surface, the silanised LPGs were immersed in 25mM DMS in phosphate buffered saline solution (PBS) for 35min at room temperature. Then the activated LPGs were rinsed by DI water three times and dried in the air.

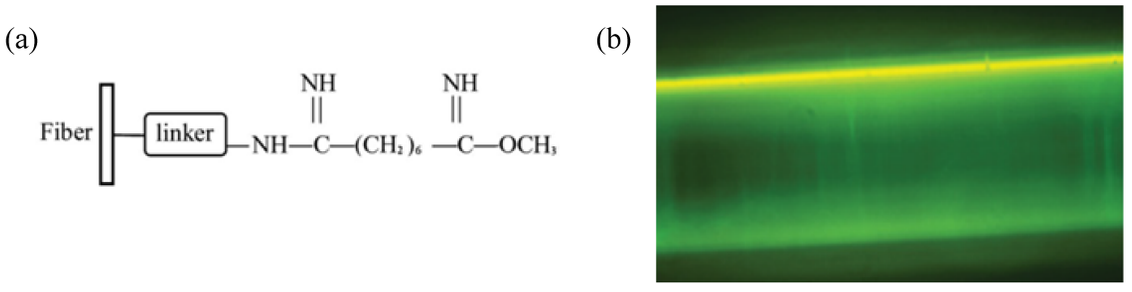

Figure 22. (a) Activation of the silanised glass surface using DMS. (b) The image of GFP fluorescence on the fibre surface;

GFP Immobilisation and Fluorescent Test: In order to provide a simple method to determine whether biomolecules are able to be successfully immobilised on the fibre glass surface, Green Fluorescent Protein (GFP), which is an intrinsically fluorescent protein that has been used extensively as a tool in biology to enable imaging, was employed to detect the attachment of protein onto the fibre surface. A DMS activated fibre, as described above, was incubated in 1mg/ml GFP in PBS for 16hrs at room temperature. The GFP-deposited fibre surface was observed under optical microscope with UV light source using appropriate filters for GFP fluorescence detection and the image was captured and shown in Fig. 22(b), exhibiting successful protein immobilisation.

Immobilisation of Probe DNA: The immobilisation process was carried out by incubation of an activated LPG in 1μM probe DNA (as shown in Table 2) in PBS for 16hrs at room temperature. The spectra of LPG as shown in Fig. 23(a) were measured at the beginning and end of the immobilisation process, respectively, by OSA with a resolution of 0.1nm. The grating wavelength was defined by the centroid calculation method. After 16hrs deposition, a blue-shift in wavelength of 254pm was observed, showing the fibre surface has been modified successfully.

Oligonucleotide	5′ end modification	Sequence	3′ end modification
Probe	none	GCA CAG TCA GTC GCC	NH_2
Target	none	GGC GAC TGA CTG TGC	none

Table 2. Sequences and modifications of the Probe and Target Oligonucleotides.

Hybridisation of Target DNA: Hybridisation was executed with target DNA. After cleaning with DI water, the grating sensor was rinsed in 6xSSPE (0.9M NaCl, 0.06M NaH_2PO_4, and 0.006M EDTA) then immersed in fresh 1μM target DNA in 6xSSPE buffer for 60min at room temperature. The grating wavelength shift, as shown in Fig. 23(b), was monitored *in situ* through whole hybridisation process. An increase of 715pm was observed in wavelength from the start of hybridisation process until the end and most of the change takes place in the first 20min showing that hybridisation takes place very quickly. Hybridisation of target DNA has been monitored successfully in real-time by this grating sensor.

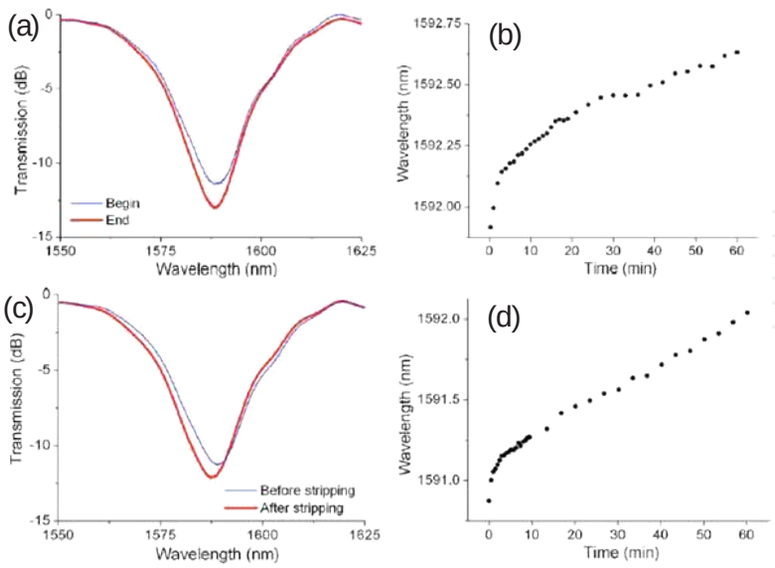

Figure 23. (a) Spectra of biosensor before and after probe DNA immobilisation; (b) Wavelength evolution of biosensor against time during the hybridisation of target DNA; (c) Spectra of biosensor before and after the stripping procedure; (d) Wavelength shift against time during the re-hybridisation process.

Stripping Procedure and Reusability: For re-use, grating sensor was incubated in a freshly prepared stripping buffer of 5mM Na_2HPO_4 and 0.1%(w/v) Sodium dodecyl sulfate (SDS) at 95°C for 30s, three times, then was washed with DI water and dried for the re-hybridisation. The grating spectra, as shown in Fig. 23(c), were measured in DI water before and after the stripping procedure. A blue-shift of 1257pm has been observed, which is caused by the stripping procedure. After stripping, the sensor was re-hybridised by immersion in 2μM target DNA in 6xSSPE buffer for 60min at room temperature. A 1165pm wavelength increase has been measured, as shown in Fig. 23(d), demonstrating the re-usability of the LPG biosensor.

A novel optical biosensor based on LPG has been demonstrated and used for detection of DNA hybridisation. A change of wavelength of 1165pm was observed in the 60min hybridisation of target DNA, showing a significantly higher sensitivity than the reported biosensor based on core-etched FBG [57].

5. Conclusions

In-fibre grating technology has developed very rapidly in recent years and the range of its applications will continue to grow, such as biomedical, biosensing, environmental monitoring and health care. This chapter, we have reviewed the theory, the fabrication techniques and the types of fibre gratings. In addition we have demonstrated the success of grating based devices for chemical and bio- sensing. It may be possible to further enhance the sensitivity by selecting the special fibre such as D-fibre, by refining the etching process, or by designing integrated microfluidic channels [61] or by developing the novel grating structures [62]. We are also interested in developing the new biosensor for selective bio-sensing, such as protein-protein, protein-DNA and protein-substrate interaction.

Acknowledgements

I gratefully acknowledge Professor Ian Bennion, Professor Lin Zhang, and Dr. Anna V. Hine et al. at Aston University, United Kingdom, for their contributions in many relevant works presented in this chapter.

Author details

Xianfeng Chen*

Address all correspondence to: x.chen@bangor.ac.uk

School of Electronic Engineering, Bangor University, Bangor, United Kingdom

References

[1] A. Yariv, "Coupled-mode theory for guided-wave optics," *IEEE J. Quantum Electron.*, 9, 919-933, 1973.

[2] K. O. Hill, Y. Fujii, D. C. Johnson, and B. S. Kawasaki, "Photosensitivity in optical fiber waveguides: Application to reflection filter fabrication," *Appl. Phys. Lett.*, 32, 647-649, 1978.

[3] T. Erdogan, "Fiber grating spectra," *J. Lightwave Technol.* 15, 1277-1294, 1997.

[4] I. Bennion, J. A. R. Williams, L. Zhang, K. Sugden, and N. J. Doran, "UV-written in-fibre Bragg gratings," *Optical and Quantum Electronics*, 28, 93-135, 1996.

[5] L. Zhang, W. Zhang, and I. Bennion, "In-fiber grating optic sensors," in *Fiber Optic Sensors*, F. T. S. Yu and S. Yin eds., 123-181, Marcel Dekker, New York, 2002.

[6] A. Othonos and K. Kalli, Fiber Bragg gratings, Artech House, Inc. 1999.

[7] R. Kashyap, Fiber Bragg gratings, Academic Press, 1999.

[8] T. Erdogan, and J. E. Sipe, "Tilted fiber phase gratings," *J. Opt. Soc. Am.A*, 13,296-313, 1996.

[9] H. Kogelnik, and C. W. Shank, "Coupled wave theory of distributed feedback lasers," *J.Appl.Phys.*, 43, 2327-2335, 1972.

[10] T. Erdogan, "Cladding-mode resonances in short- and long- period fiber grating filters," *J. Opt. Soc. Am. A*, 14, 1760-1773, 1997.

[11] A. M. Vengsarkar, P. Lemaire, J. Judkins, V. Bhatia, T. Erdogan, and J. Sipe, "Long-period fiber gratings as band-rejection filters," *J. Lightwave Technol.*, 14, 58-65, 1996.

[12] V. Bhatai and A. M. Vengsarkar, "Optical fiber long-period grating sensors," *Opt. Lett.*, 21, 692-694, 1996.

[13] K. Lee, and T. Erdogan, "Fiber mode coupling in transmissive and reflective tilted fibre gratings," *Appl. Opt.*, 39, 1394-1404, 2000.

[14] G. Meltz, W. W. Morey, and W. H. Glenn, "Formation of Bragg gratings in optical fibers by transverse holographic method," *Opt. Lett.*, 14, 823-825, 1989.

[15] L. Zhang, K. Sugden, J. A. R. Williams, and I. Bennion, "Postfabrication exposure of a gap-type bandpass filters in broadly chirped fiber gratings," *Opt. Lett.*, 20(18), 1927-1929, 1995.

[16] K. Sugden, I. Bennion, A. Molony, and N. J. Copner, "Chirped gratings produced in photosensitive optical fibers by fiber deformation during exposure," *Electron.Lett.*, 30(5), 440-442, 1994.

[17] K. C. Byron, K. Sugden, T. Bricheno, and I. Bennion, "Fabrication of chirped Bragg gratings in photosensitive fiber," *Electron. Lett.*,29(18), 1659-1660, 1993.

[18] J. Albert, K. O. Hill, B. Malo, S. Theriault, F. Bilodeau, D. C. Johnson, L. E. Erickson, "Apodization of the spectral response of fiberbragg gratings using a phase mask with variable diffraction efficiency," *Electron. Lett.*,31(3), 222-223, 1995.

[19] J. Albert, K. O. Hill, D. C. Johnson, F. Bilodeau, and M. J. Rooks, "Moire phase masks for automatic pure apodisation of fiber Bragg gratings," *Electron. Lett.*,32(24), 2260-2261, 1996.

[20] R. Kashyap, P. F. Mckee, and D. Armes, "UV written reflection grating structures in photosensitive optical fibers using phase-shifted phase mask," *Electron. Lett.*,30(23), 1977-1978, 1994.

[21] J. Canning and M. G. Sceats, "_ phase shifted periodic distributed structures in optical fibers by UV post-processing," *Electron.Lett.*,30(16), 1344-1345, 1994.

[22] L. Zhang, K. Sugden, I. Bennion, and A. Molony, "Wide-stopband chirped fibermoire grating transmission filters," *Electron. Lett.*,31(6), 477-479, 1995. 184

[23] S. Legoubin, E. Fertein, M. Douay, P. Bernage, P. Niay, F. Bayon, T. Georges, "Formation of moire grating in core of germanosilicatefiber by transverse holographic double exposure method," *Electron. Lett.*,27(21), 1945-1946, 1991.

[24] B. J. Eggleton, P. A. Krug, L. Poladian, and F. Ouellette, "Long periodic superstructure Bragg gratings in optical fibers," *Electron. Lett.*,30(19), 1620-1622, 1994.

[25] M. Durkin, M. Ibsen, M. J. Cole, R. I. Laming, "1m long continuously-written fibre Bragg gratings for combined second- and third-order dispersion compensation," *Electron.Lett.*,33(22), 1891- 1893, 1997.

[26] S. J. Mihailov, T. J. Stocki, and D. C. Johnson, "Fabrication of tilted fibre-grating polarisation-dependant loss equaliser," *Electron. Lett.*,37, 284 -286, 2001.

[27] K. Zhou, A. Simpson, X. Chen, L. Zhang, and I. Bennion, "Radiation mode out-coupling from blazed FBGs and its spatial-to-spectral encoding function investigated by side-tap detection," *Bragg Gratings, Poling and Photosensitivity (BGPP-2003),* 2003.

[28] J. Peupelmann, E. Krause, A. Bandemer, and C. Schäffer, "Fibre-polarimeter based on grating taps," *Electron.Lett.*,38, 1248-1250, 2002.

[29] S. L. Mihailov, R. B. Walker, T. J. Stocki, and D. C. Johnson, "Fabrication of tilted fibre-grating polarisation-dependent loss equaliser," *Electron. Lett.*,37, 284-286, 2001.

[30] P. I. Reyes and P. S. Westbrook, "Tunable PDL of Twisted-Tilted Fiber Gratings," *IEEE Photon. Technol. Lett.*, 15, 828-830, 2003.

[31] K. Zhou, X. Chen, A. G. Simpson, L. Zhang, and I. Bennion, "High extinction ratio in-fiber polarizer based on a 45°-tilted fiber Bragg grating," in *Optical Fibre Communication Conference*, (Anaheim, California), paper OME22, 2005.

[32] K. Zhou, G. Simpson, X. Chen, L. Zhang, and I. Bennion, "High extinction ratio in-fiber polarizers based on 45°-tilted fiber Bragg gratings," *Opt. Lett.* 30, 1285-1287, 2005.

[33] Z. Yan, C. Mou, K. Zhou, X. Chen, and L. Zhang, "UV-inscription, polarization- dependant loss characteristics and applications of 45° tilted fiber gratings", *J. Lightwave Technol.*, Vol. 29(18), 2715-2724, 2011.

[34] X. Shu, L. Zhang, and I. Bennion, "Sensitivity characteristics near the dispersion turning points of long-period fiber gratings in B/Gecodopedfiber", *Opt. Lett.,* 26, 1755-1757, 2001.

[35] X. Shu, L. Zhang, and I. Bennion, "Sensitivity characteristics of Long-period fibre gratings", *J. Lightwave Technol*., 20, 255-266, 2002.

[36] D. J. Webb, M. W. Hathaway, D. A. Jackson, S. Jones, L. Zhang, and I. Bennion, "First in-vivo trials of a fiber Bragg grating based temperature profiling system," *J. Biomed. Opt*., 5, 45-50, 2000.

[37] Z. Zhang and J. S. Sirkis, "Temperature-compensated long period grating chemical sensor, " *Proc. Int. Conf. Optical Fiber Sensors (OFS'12),* Williamsburg, VA, 294-297, 1997.

[38] H. J. Patrick, A. D. Kersey, and F. Bucholtz, "Analysis of the response of long period fiber gratings to external index of refraction," *J. Lightwave Tech.*, 16, 1606-1611, 1998.

[39] X. Chen, K. Zhou, L. Zhang, and I. Bennion, "Simultaneous measurement of temperature and external refractive index by use of a hybrid grating in D-fibre with enhanced sensitivity by HF etching," *Appl. Opt*., 44, 178-182. 2005.

[40] X. Chen, K. Zhou, L. Zhang, and I. Bennion, "Optical chemsensor based on etched tiled Bragg grating structures in multimode fiber", *IEEE Photon. Technol. Lett*., 17, 864-866. 2005.

[41] X. Chen, K. Zhou, L. Zhang, and I. Bennion, "Optical chemsensors utilizing long-period fiber gratings UV-inscribed in D-fiber with enhanced sensitivity through cladding etching," *IEEE Photon. Technol. Lett*., 16, 1352-1354. 2004.

[42] X. Chen, K. Zhou, L. Zhang, and I. Bennion, "High sensitivity biosensors based on dual-peak LPGs sensitised by light cladding etching," *17th International Conference on Optical Fibre Sensors (OFS-2005)*, Proc. SPIE 5855, 383-386, Belgium, 2005.

[43] X. Chen, K. Zhou, M. Hughes, E. Davies, L. Zhang, A. Hine, K. Sugden, and I. Bennion, "DNA hybridisation biosensor based on dual-peak long-period grating", *AOE2007*, pp. 87-89, China, Oct.17-19, 2007.

[44] X. Chen, L. Zhang, K. Zhou, E. Davies, K. Sugden, I. Bennion, M. Hughes, and A. Hine, "Real-time detection of DNA interactions with long-period fiber-grating-based biosensor", *Opt. Lett*., Vol. 32 (17), 2541-2543, 2007.

[45] A. Hine, X. Chen, M. D. Hughes, K. Zhou, E. Davies, K. Sugden, I. Bennion, and L. Zhang, "Optical fibre-based detection of DNA hybridization", *Biochem. Soc. Trans.*Vol.37, 445-449, 2009

[46] Meltz, W. W. Morey, and J. R. Dunphy, "Fiber Bragg grating chemical sensor," in *Chemical, biochemical, and Environmental Fiber Sensor III*, Proc. SPIE (Int. Soc. Opt. Eng.) 1587, 350-361, 1991.

[47] K. Schroeder, W. Ecke, R. Mueller, R. Willsch, and A. Andreev, "A fiber Bragg grating refractometer," *Meas. Sci, Technol.*, 12, 757-764, 2001.

[48] W. Liang, Y. Y. Huang, Y. Xu, R. K. Lee, and A. Yariv, "Highly sensitive fiber Bragg grating refractive index sensors," *Appl. Phys. Lett*., 86, 151122, 2005.

[49] K. S. Chiang, Y. Liu, M. N. Ng, and X. Dong, "Analysis of etched long-period fibre grating and its response to external refractive index," *Electron.Lett.*,36, 966-967, 2000.

[50] S. Kim, Y. Jeong, S. Kim, J. Kwon, N. Park, and B. Lee, "Control of the characteristics of a long-period grating by cladding etching," *Appl. Opt.*, 39, 2038-2042, 2000.

[51] T. Volotinen, W. Griffoen, M. Ganonna, and H. G. Limberger, Eds., Reliability of optical fiber and components-final report of COST 246, London, U. K: Springer-Verlag, 1999.

[52] D. R. Lide, Ed., CRC Handbook of Chemistry and Physics, CRC Press, Boca Raton, 1999.

[53] H. R. Luckarift, J. C. Spain, R. R. Naik, and M. O. Stone, "Enzyme immobilization in a biomimetic silica support," *NatureBiotechnol.*, 22, 211-213, 2004.

[54] M. Beier and J. D. Hoheisel, "Versatile derivatisation of solid support media for covalent bonding on DNA-microchips," *Nucleic Acids Res.*, 27, 1970-1977, 1999.

[55] A. Ksendzov and Y. Lin, "Integrated optics ring-resonator sensors for protein detection," *Opt. Lett*., 30, 3344-3346, 2005.

[56] A. N. Chryssis, S. M. Lee, S. B. Lee, S. S. Saini, and M. Dagenais, "High sensitivity evanescent field fiber Bragg grating sensor," *IEEE Photon. Technol. Lett.,* 17 (6), 1253-1255, 2005.

[57] A. N. Chryssis, S. S. Saini, S. M. Lee, H. Yi, W. E. Bentley, and M. Dagenais, "Detecting hybridization of DNA by highly sensitive evanescent field etched core fibre Bragg grating sensors," *IEEE Journal of Selected Topics in Quantum Electronics*, 11 (4), 864-872, 2005.

[58] M. P. DeLisa, Z. Zhang, M. Shiloach, S. Pilevar, C. C. Davis, J. S. Sirkis, and W. E. Bentley, "Evanescent wave long-period fiber Bragg grating as an immobilized antibody biosensor," *Anal. Chem.*, 72, 2895-2900 (2000).

[59] Hand, E. S. and Jencks, W. P. Mechanism of the reaction of imidoesters with amines. *J. Am. Chem. Soc*., 84, 3505-3514 (1962).

[60] Mattson, G., Conklin, E., Desai, S., Nielander, G., Savage, D., and Morgensen, S. A practical approach to crosslinking.*Mol. Biol. Rep*., 17, 167-183 (1993).

[61] K. Zhou, Y. Lai, X. Chen, K. Sugden, L. Zhang, and I. Bennion, "A refractometer based on a micro-slot in a fiber Bragg grating formed by chemically assisted femtosecond laser processing", *Opt. Express*, Vol. 15 (24), 15848-15853, 2007

[62] X. Chen, K. Zhou, A. Adebayo, and L. Zhang, "Chemical sensor using Mach-Zehnder interferometer based on a pair of largely tilted fibre gratings", *2012 Bragg Gratings, Photosensitivity and Poling in Glass Waveguides (BGPP-2012) Topical Meeting*, JTu5A.51, Colorado, USA, 17-21 June 2012

IntechOpen